Organic Electronics 39 (2016) 279–287

Contents lists available at ScienceDirect

Organic Electronics

journal homepage: www.elsevier.com/locate/orgel

Diketopyrrolopyrrole based highly crystalline conjugated molecules for application in small molecule donor-polymer acceptor nonfullerene organic solar cells

Jianyu Yuan*, Wanli Ma**

Institute of Functional Nano & Soft Materials (FUNSOM), Jiangsu Key Laboratory for Carbon-Based Functional Materials & Devices, Soochow University, 199 Ren-Ai Road, Suzhou Industrial Park, Suzhou, Jiangsu, 215123, PR China

ARTICLE INFO

Article history:
Received 18 September 2016
Received in revised form
13 October 2016
Accepted 13 October 2016

Keywords:
Nonfullerene solar cells
Donor crystallinity
Morphology
Mobilities

ABSTRACT

In order to specifically investigate the low efficiency of small molecule donor-polymer acceptor (M-P) nonfullerene organic solar cells, we have successfully modify the synthesis of a series of D-π-A-π-D conjugated molecules containing diketopyrrolopyrrole (DPP) and different end groups. By incorporation of end group with different size of π-conjugation (benzene, naphthalene and pyrene), we further improved the fill factor (*FF*) and short current density (J_{sc}) of the donors molecule. Our experimental results and theoretical calculations have proven that the size of the end groups can influence the molecule crystallinity, mobility and intermolecular packing by altering the molecular coplanarity. As the result of improved crystallinity, morphology and fine-tuned mobilities, we demonstrated an increased FF, a high J_{sc} of ~4.5 mA/cm^2 and a power conversion efficiency of 2.05%, which is among the highest efficiency reported for M-P nonfullerene solar cells. Our results provide opportunities and possibilities of achieving higher performance M-P nonfullerene solar cells in the future.

© 2016 Elsevier B.V. All rights reserved.

1. Introduction

Organic solar cells made of solution-processed bulk heterojunction (BHJ) organic materials are potential low-cost alternatives for renewable energy generation [1]. During the past decade, synergistic efforts in donor materials (small molecules, oligomers, polymers) design and device processing optimization have rapidly increased the power conversion efficiencies (PCEs) of organic photovoltaic (OPV) that approach 12% [2]. However, fullerenes are not ideal acceptor materials due to many intrinsic issues, such as weak light absorption, almost fixed chemical structure and energy levels [3], further limiting the open-circuit voltage (V_{oc}) and short-circuit current density (J_{sc}) of these solar cell devices. Furthermore, the inherent tendency of fullerene to aggregate under elevated temperatures has been considered a key factor for deteriorated morphology and consequently reduced lifetime of PSCs [4]. Therefore, despite the tremendous achievements to date, the research development of OPVs has reached the stage where the scalability of the materials, stability and cost need to be further optimized before reaching the threshold for large-scale commercialization [5].

Functional photovoltaic materials applied into organic solar cells are usually synthesized via the *Suzuki*, *Stille* or *Negishi* cross-coupling reactions, which involve the preparation of organo-boron, organo-tin or organo-zinc reagents, respectively [6]. In recent years, attributing to the great progress of C-H activation reaction, thiophene has been regarded as an ideal moiety in synthetic organic chemistry for direct arylation with aryl halides due to the ease of palladation through a concerted metalation deprotonation pathway [7]. These reactions possess numerous advantages [8] over traditional cross-coupling reactions such as: (a) avoidance of the use of organometallic reagents in the starting materials leading to simpler by products and higher atom economy, (b) fewer synthetic steps, (c) higher yields, (d) better compatibility with chemically sensitive functional groups, and (e) the scalability preparation of the target conjugated materials.

Meanwhile, solution-processed organic solar cells (OSCs) using a nonfullerene electron acceptor has been rapidly improved relative to the fullerene counterparts, with PCE past 11% up to date [9]. Typically, the nonfullerene OSCs can be divided into four different

* Corresponding author.
** Corresponding author.
E-mail addresses: jyyuan@suda.edu.cn (J. Yuan), wlma@suda.edu.cn (W. Ma).

http://dx.doi.org/10.1016/j.orgel.2016.10.021
1566-1199/© 2016 Elsevier B.V. All rights reserved.

types: polymer donor-small molecule acceptor (P-M) [9], polymer donor-polymer acceptor (P-P) [3c,10], small molecule donor-small molecule acceptor (M-M) [11] and small molecule donor-polymer acceptor (M-P) [12]. However, among these nonfullerene OSCs, the development of small molecule donor-polymer acceptor system has lagged significantly behind in device performance. So far, only a few reported M-P OSCs exhibited power conversion efficiencies (PCEs) above 2% [12], with the very recent two ones reaching 4.5% [12b,13]. The lower PCEs of M-P OSCs are generally hypothesized to the large polymer phase separation, relatively low electron mobility of polymer acceptors and the inefficient charge dissociation at the donor/acceptor (D/A) interface [12a,14]. However, it is worth noting that few previous works have been focused on the effect of initial donor molecules properties on the relevant M-P OSCs performance. We should realize that the subtle changes in donor molecular structure may also have significant impact on the material optoelectronic properties, processing parameters, blend morphology, and the resulting solar cell characteristics selection. Especially, the morphology change is critical to the device performance.

In this contribution, a series of low band-gap donor molecules (DPP-B, DPP-N and DPP-P) sharing similar D-π-A-π-D backbone structure were synthesized via one-pot direct acylation reaction. We incorporated different end groups (benzene, naphthalene and pyrene) into the molecular backbone, in order to investigate how the subtle changes in molecular structure impact relevant optoelectronic properties and the resulting M-P nonfullerene OSCs characteristics. Finally, all these molecules were used together with a polymer acceptor P(NDI2OD-T2) (N2200) [15] in M-P nonfullerene solar cells. As shown in Scheme 1, to achieve higher intermolecular contacts, DPP-N and DPP-P were synthesized by substituting the benzene end-group with naphthalene and pyrene, aiming to enhance charge carrier mobility and light absorption of donor molecules. The properties of these molecules were systematically studied by UV–vis absorption, Density Functional Theory (DFT) simulation and 2D grazing incidence wide-angle X-ray scattering (GIWAXS). The corresponding M-P nonfullerene solar cells were also fabricated to investigate the effect of molecular structure on the device photovoltaic performance. We revealed that the structure change of small molecule donor acceptor can adjust the molecular ordering and crystallinity in solid film, resulting in significantly different performance. The optimized M-P nonfullerene solar cells based on DPP-P/N2200 shows a relatively high J_{sc} of ~4.5 mA/cm2 (0.69 mA/cm2 for DPP-B/N2200 and 1.14 mA/cm2 for DPP-N/N2200), and a high PCE of 2.05% (0.20% for DPP-B/N2200 and 0.50% for DPP-N/N2200). More importantly, our results suggest that small molecule donor with higher crystallinity can be designed for creating better charge transport and blend morphology in M-P nonfullerene OSCs.

2. Results and discussion

2.1. Synthetic procedures

The structure and synthetic route of the donor molecules are illustrated in Scheme 2. The detailed procedure is described in the experimental part. All molecules were prepared via direct arylation reaction [16], using a phosphine-free catalytic system, and the reaction could be accelerated greatly with high yields (>90%) in the presence of pivalic acid (PivOH). Former reports demonstrated the preparation procedure of these DPP-based materials using Palladium(Pd)-assisted Suzuki cross-coupling reaction with multiple steps [17], however, the highly efficient one-pot synthesis of these functional materials in this contribution gives us a promising prospect for easier scale up production. These advantages make the direct arylation protocol an ideal and versatile strategy for the synthesis of structural complicated DPPs that may possess chemically sensitive functionalities. Herein, all the DPP molecules materials exhibit good solubility in common solvents at room temperature, like chloroform (CF), chlorobenzene (CB) and *o*-dichlorobenzene (ODCB).

2.2. Optical properties

UV–vis absorption spectra of DPP-based molecules and N2200 are shown in Fig. 1. The molecular solutions in chloroform display board absorption from 450 to 680 nm. For DPP-N and DPP-P, both solutions show distinct shoulder peaks next to the absorption maximum in their solutions, which is typical for DPP based molecules. We noticed that the absorption in region of 400–600 nm of DPP-N and DPP-P are almost the same, indicating the similar intramolecular charge transfer (ICT) between the donor and

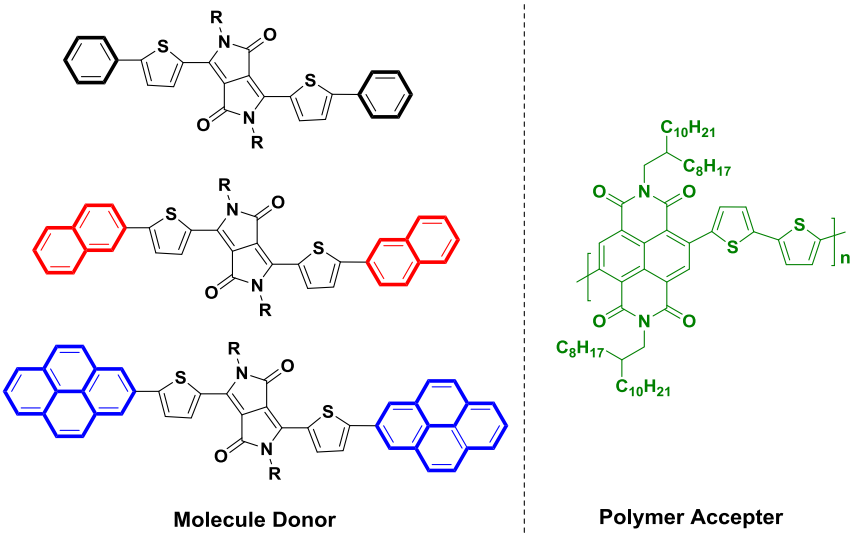

Scheme 1. Molecular structures of donor and acceptor.

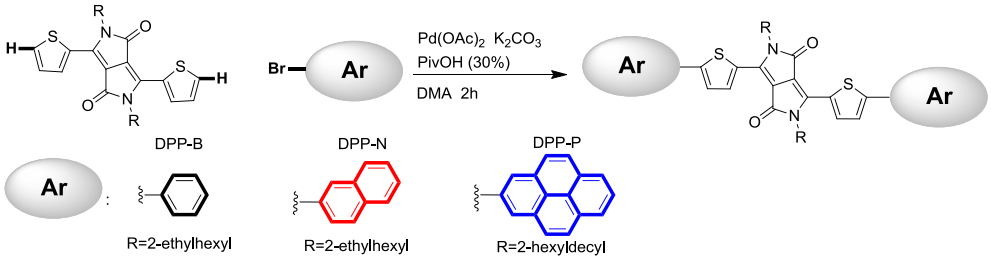

Scheme 2. Synthetic access to DPP-B, DPP-N and DPP-P via one-pot direct arylation reaction.

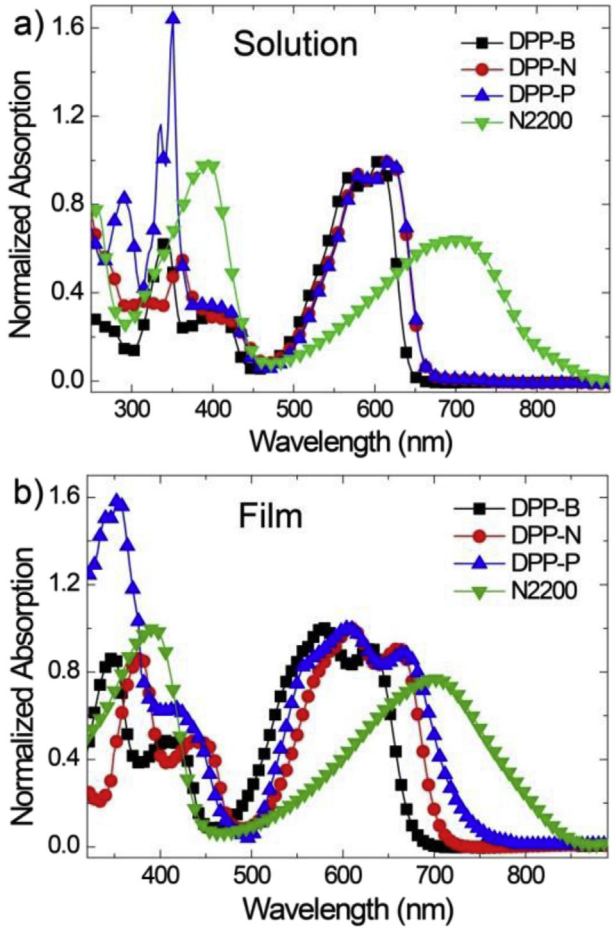

Fig. 1. Absorption spectra of solutions in chloroform at room temperature (a) and thin films cast from chloroform solutions (b).

acceptor units [6a]. Blue-shift absorption is observed in DPP-B between compared to DPP-N and DPP-P in both solution and solid state, indicating the weaker ICT when adopting benzene as the end-groups. Besides, the absorption below 400 nm was notably enhanced in both solution and solid state when incorporating larger π-conjugated pyrene as the end-groups. Thin film absorption spectra of DPP-B, DPP-N and DPP-P exhibit similar trend compared to that in solutions. The optical band gap (E_g) of DPP-B, DPP-N and DPP-P is 1.82 eV, 1.75 eV and 1.66 eV, respectively, as determined by the onset of film absorption. It is speculated that different degree of molecular packing was formed in solid state, likely due to different molecular geometry and intermolecular contacts. UV–vis absorption spectra of polymer acceptor N2200 are also shown in Fig. 1. Compared to the fullerene acceptors, the absorption of N2200 is greatly improved, exhibiting a narrow optical band-gap of 1.46 eV. Herein, the small molecule donor-polymer acceptor nonfullerene blend extends the absorption into the near-infrared regions of the solar spectrum, which could potentially contribute to photocurrent. And theoretically obtain larger J_{sc} values with only thin films.

2.3. Theoretical calculations and structural order in solid films

DFT calculations for molecules using Gaussian 09 at the level of B3LYP/6-31g(d) were performed [18], aiming to gain insight into the possible molecular geometries arising from the chemical structures. To simplify the calculations, the alkyl chains attached on DPP moiety were replaced by CH_3 groups. In Fig. 2, our calculations indicate that the dihedral angles are −27.8°, 31.0°, 33.6° and −23.4° for DPP-B, -22.9°, 11.7°, 15.8° and −21.3° for DPP-N and −2.5°, 9.2°, 10.8° and −4.8° for DPP-P. The obviously smaller dihedral angles of DPP-P than DPP-N and DPP-B imply a better planarity, which will help to improve the intermolecular packing, resulting in reduced optical band-gap and improved charge transport. These results theoretically proved the proper selection of end groups can efficiently modify the molecular structures of the DPP-based linear molecules. We also calculated the materials' energy levels to investigate how the subtle changes in molecular structure impact relevant electronic properties. Due to the incorporation of strong electron-deficient moiety DPP as the core, the LUMO energy levels will be mainly decided by the acceptor block in D-A materials [19]. On the other hand, all benzene, naphthalene and pyrene units exhibit relatively weak electron-donating ability, as shown in Fig. 2, no obvious difference is observed in the calculated LUMO, HOMO energy levels.

Grazing incidence wide-angle X-ray scattering (GIWAXS) measurements were performed to investigate the relevant structure information in solid state [20]. We first investigated the effect of end group on the polymer order in film. As shown in Fig. 3, the 2D GIWAXS patterns of a DPP-N and DPP-P thin film shows sharply defined rings and peaks, suggesting that the packing of DPP-P is both more crystalline and more aligned than that of DPP-B, whose scattering pattern indicate relatively amorphous films. According to previous report [17b], DPP-P shows a closely-packed, interdigitated crystal structure with extensive overlap of C2-pyrene moieties. The interplanar distance between two pyrene units is as short as 3.50 Å, confirming strong interaction between molecules. All these results exhibit similar trend with the DFT simulation, the pyrene end group with extended π-conjugation can direct favourable packing configuration for charge transport. In addition, the polymer acceptor N2200 also exhibit more ordered solid structure compared to other conjugated polymers, a broad and relatively strong diffraction peak appeared in the out-of-plane direction, which corresponds to a preferable face-on packing orientation for the polymer in the films, and the corresponding "π–π stacking" distance is ~4.0 Å. It has been presumed that the generation and

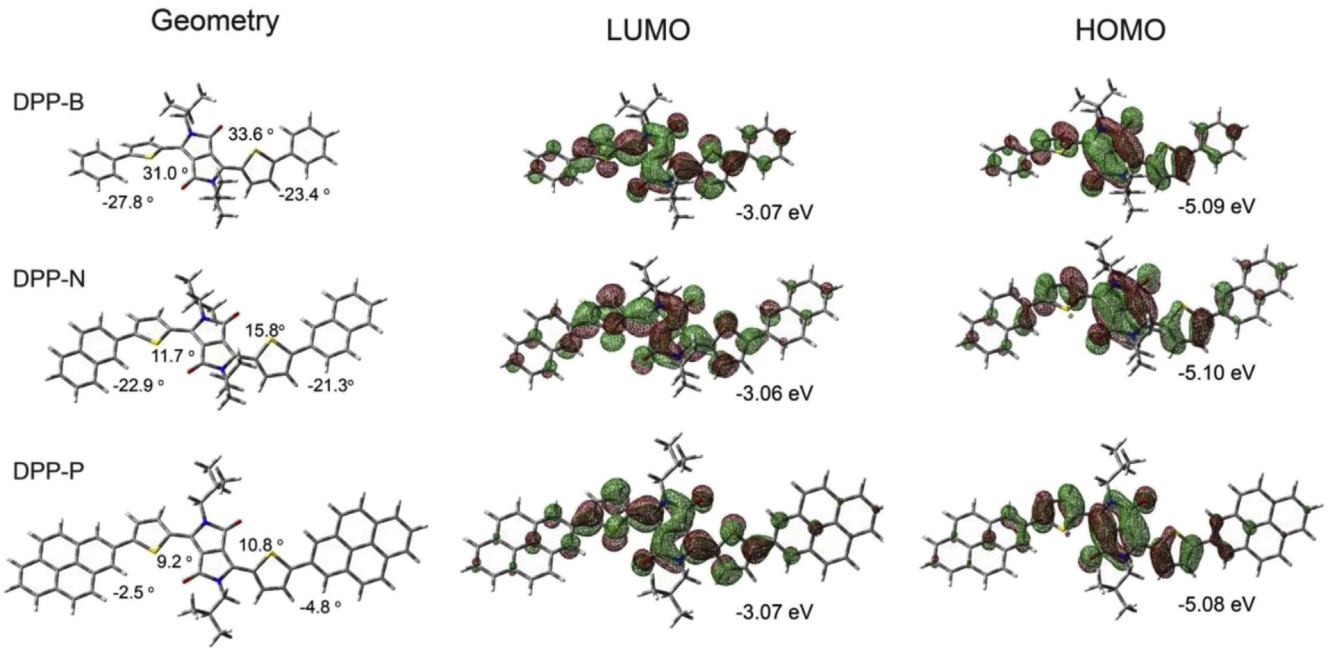

Fig. 2. Optimized molecular geometries and LUMO, HOMO energy levels obtained by DFT calculation.

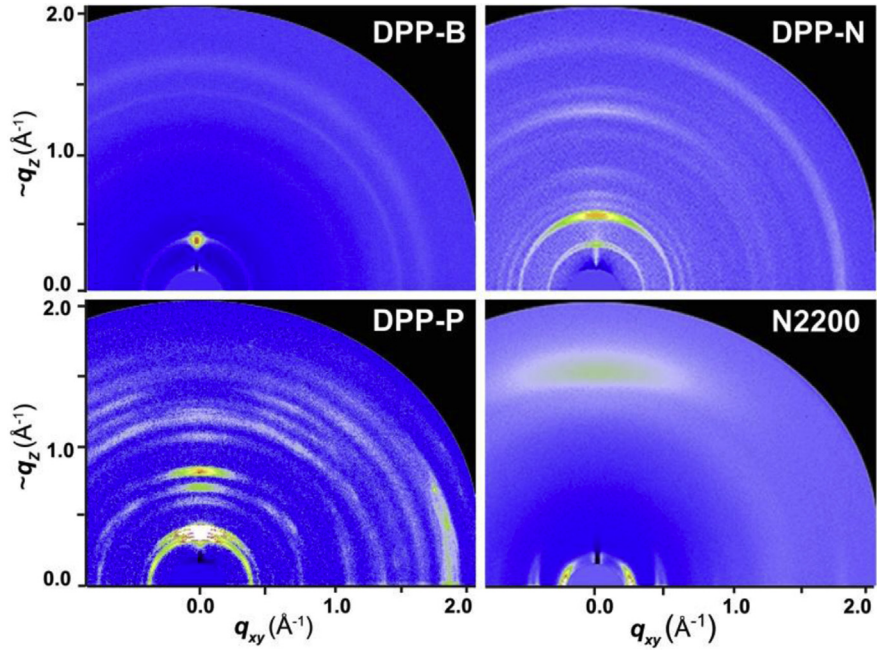

Fig. 3. 2D-GIWAXS patterns of DPP-B, DPP-N, DPP-P and N2200 thin films.

dissociation of free charge carriers is dictated by the microscopic structure of the donor and acceptor at the heterojunction in very anisotropic nonfullerene system [21]. A proper crystal orientation and degree of crystallinity in polymer domains is a prerequisite for efficiently dissociating electron-hole pairs into free charge carriers [22].

2.4. Solar cell performance

Nonfullerene BHJ OSCs were fabricated using DPP molecules as donor and N2200 as the electron acceptor. The structure is ITO/PEDOT:PSS (40 nm)/blend/Al (80 nm), and the device area is 7.25 mm^2. All devices were operated under an N_2 atmosphere. Device optimization included adjustments of solvents, donor-acceptor blend ratio, post-treatment and active layer thickness. CF was eventually chosen as the best processing solvent, the optimal molecule/polymer weight ratio was determined to be 2:1, with a total solid concentration of 16 mg mL^{-1} for all small molecule donor. Thermal annealing and solvent additive 1,8-diiodooctane (DIO) has also been adopted to further enhance

device performance, since it has been proven to be an efficient and universal post-treatment to improve the morphology of polymer-fullerene films [23].

M-P BHJ blends cast from neat solvent without any treatment exhibited a PCE of 0.04%, 0.05% and 1.18% for DPP-B, DPP-N and DPP-P, respectively, with corresponding V_{oc} values of 0.85 V, 0.74V and 0.88 V. The relatively low PCEs were due to the low J_{sc} and *FF*. As shown in Table 1, thermal annealing hardly enhances the photovoltaic performance in all the devices, probably due to the unfavourable self-contained morphology from the initial blend films. However, as shown in Table 1 and Fig. 4c, significant improvements were observed upon introduction DIO as a solvent additive to the processing solvent, giving highest PCEs of 0.20%, 0.50% and 1.75% for DPP-B, DPP-N and DPP-P, respectively. The enhancement of PCEs was mainly due to the improved J_{sc} and *FF*. Finally, we realized a highest PCE of 2.05% for DPP-P/N2200 solar cell device through the synergistic effect between thermal annealing and solvent additive, which is also among the highest report for the less focused M-P nonfullerene solar cells [12,13]. External quantum efficiency (EQE) curves are shown in Fig. 4d. All M-P devices show a broad EQE response from 300 to 800 nm, however, DPP-B/N2200 and DPP-N/N2200 exhibit average value less than 5% across the 500–750 nm range. In contrast, DPP-P/N2200 display quite higher quantum efficiency values, with maximum EQE value over 30% and the J_{sc} values calculated from integration of the EQE with the AM1.5G reference spectrum are in agreement (±5%) with the Jsc obtained from the *J-V* measurements.

In order to understand the major effect on small molecule donor properties on device performance, we carried out several investigations on charge extraction, generation and transport. The dependence of the photocurrent density (J_{ph}) on the effective voltage (V_{eff}) was firstly recorded under illumination at 100 mWcm^{-2}. J_{ph} is equal to J_L-J_D, where J_L and J_D are the measured current under illumination and in dark, respectively. V_{eff} is equal to V_0-V_a where V_0 is the voltage when J_{ph} is zero and V_a is the applied voltage [24]. As shown in Fig. 5a, at low effective voltage below 0.5 V, the J_{ph} of DPP-P/N2200 increases drastically and reaches a plateau at higher voltage, suggesting that free charges are swept out efficiently. In comparison, the J_{ph} of DPP-B/N2200 and DPP-N/N2200 increase with a slower rate, indicating less efficient carrier extraction. More importantly, the J_{ph} of the latter is significantly smaller than that of the DPP-P/N2200 at normal device operational voltage, which is in accordance with its lower J_{sc} value. Thus the low J_{ph} density suggests that the carrier generation process for DPP-B and DPP-N must be less efficient than that of DPP-P/N2200 system, which may attributed to the different blend morphology.

The charge carrier mobility is another important factor that affects solar cell device performance. In addition, both the electron and hole mobility are crucial to achieve efficient and balanced carrier transport. To compare the charge transport properties of molecule/N2200 blends, hole only and electron-only diodes were fabricated and measured [25], with a device structure of ITO/PEDOT:PSS (40 nm)/blend/MoOx (6 nm)/Ag(80 nm) and ITO/ZnO (40 nm)/blend/LiF (0.6 nm)/Al (80 nm). As shown in Fig. 5b, the hole mobilities of the Optimized DPP-B/N2200, DPP-N/N2200 and DPP-P/N2200 blends are $1.7*10^{-6}$ cm^2 V^{-1} s^{-1}, $1.6*10^{-5}$ cm^2 V^{-1} s^{-1} and $3.2*10^{-4}$ cm^2 V^{-1} s^{-1}, respectively, which are about one order enhancement when incorporating benzene, naphthalene and pyrene into the molecular backbone as the end groups. In contrast, the *J-V* curves of electron-only devices based on the optimized DPP-B/N2200, DPP-N/N2200 and DPP-P/N2200 blends are quite similar, with SCLC fitting slope value of 5.0, 4.9 and 6.5, respectively. Further we can calculated the electron mobilities of these blend are roughly around $3.5*10^{-5}$ cm^2 V^{-1} s^{-1}, which exhibit similar value compared to the previous report for the N2200 based blend film [11,12]. Herein, all the blends exhibit quite similar electron mobilities, the major difference in hole mobilities will govern the J_{sc} and the *FF* of the M-P solar cell devices. DPP-P with enhanced crystallinity and intermolecular contacts show higher hole mobility in the BHJ blend under the same experimental condition, which proves the selection of highly crystalline small molecule donor could be an efficient approach to improve the M-P nonfullerene OSCs. However, the J_{sc} in our work (~4.5 mA/cm^2) and even in the best M-P solar cell device (~8.0 mA/cm^2) [12] is still relatively lower compared to other type nonfullerene OSCs (over 15 mA/cm^2) [9], which may probably due to the lower electron affinity, limited exciton diffusion length and higher electron traps in these polymer acceptors [12a].

Table 1
Photovoltaic properties of PSCs, under an illumination of AM1.5G, 100 mW/cm^2

	Treatment	V_{oc} (V)	J_{sc} (mA/cm^2)	*FF* (%)	*PCE* (%)
DPP-B	None	0.85	0.14	33.3	0.04
DPP-B	TA 120 °C[a]	0.69	0.06	46.9	0.02
DPP-B	0.5% DIO	0.63	0.69	43.4	0.20
DPP-N	None	0.74	0.26	27.1	0.05
DPP-N	TA 120 °C[a]	0.69	0.30	43.4	0.09
DPP-N	0.5% DIO	0.83	1.14	53.2	0.50
DPP-P	None	0.88	2.89	46.2	1.18
DPP-P	TA 120 °C[a]	0.79	3.64	45.9	1.32
DPP-P	0.5% DIO	0.78	4.47	50.3	1.75
DPP-P	0.5% DIO[b]	0.78	4.45	58.5	2.05

[a] Annealed prior to cathode deposition, 20 min.
[b] Additionally annealed at 120 °C for 3 min post to cathode deposition.

2.5. Blend morphology

Lots of previous reports [1,2] have demonstrated that the exciton dissociation and charge transport process is strongly affected by the polymer/PCBM blend morphology. Therefore, a thorough morphological study may be helpful to understand the less efficient carrier generation and transport process in nonfullerene solar cells. The morphology of DPP-B/N2200, DPP-N/N2200 and DPP-P/N2200 blend films was first examined by atomic force microscopy (AFM) (Fig. 6). By adopting different end groups to DPP-based donor molecules, the increased backbone rigidity and intermolecular contacts can promote the aggregation and crystallization process of the donor molecules. The enhanced packing and crystallinity further promote the molecular/N2200 demixing, leading to a rougher surface and large “needle” like domains (Fig. 6c). DIO is believed to allow a slower crystallization process during spin-coating, thus improving morphology through enhanced intermolecular ordering and well-developed phase separation [26]. Therefore, we observed that DPP-B/N2200 and DPP-N/N2200 blend films processed with DIO exhibited rougher surface and larger phase separation domains, which may lead to a more efficient charge transport. However, for DPP-P/N2200, the addition of DIO further enhanced the mixing the donor and acceptor domains, leading to a more uniformly distributed height surface. In order to confirm the speculation, we also investigated the blend film morphology by using GIWAXS, as shown in Fig. 7. For all the molecule/N2200 blend films, after the addition of DIO, the morphology showed a dramatic change from the original amorphous film to a semi-crystalline blend films with defined rings and peaks, the crystalline domains is the desired morphology for efficient carrier transport. However, for DPP-P/N2200, distinctive donor molecular structure has already established the strong intermolecular contacts and higher degree of structural order. Compared to DPP-B and DPP-P based blend GIWAXS patterns, the

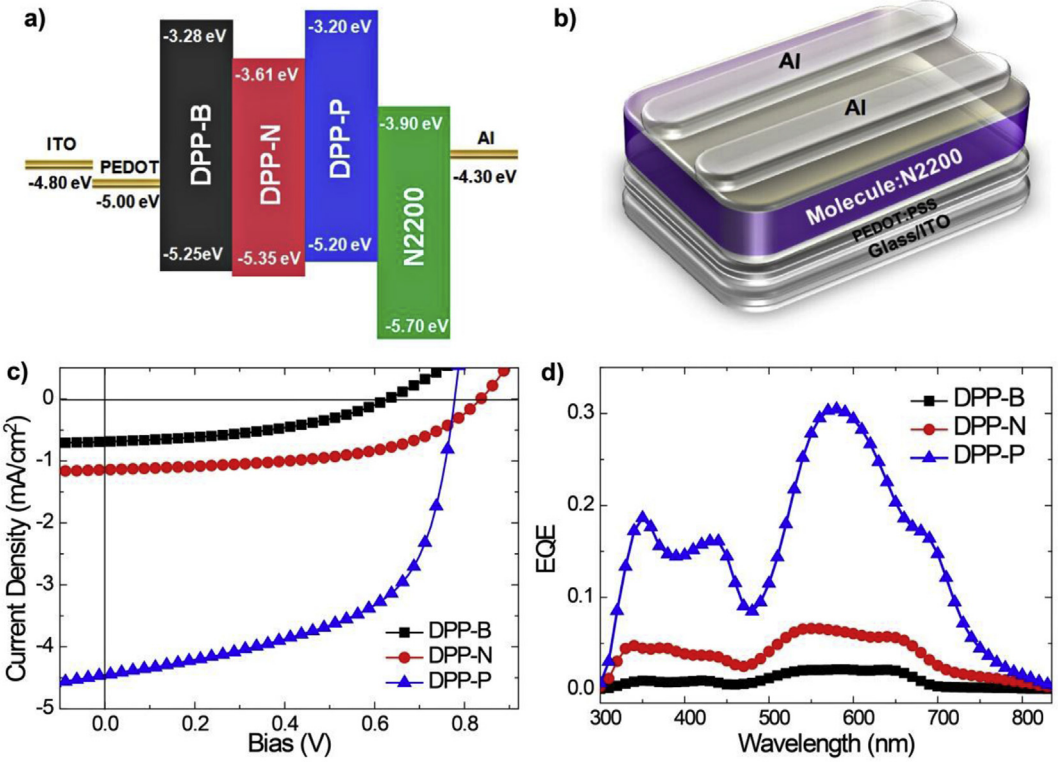

Fig. 4. Energy diagram (a) and device structures (b) of examined solar cells; (c) J-V curves of optimized molecule/N2200 based OSCs; (d) EQE plots of DPP-B, DPP-N and DPP-P based solar cells devices under optimal processing conditions.

sharply defined rings and peaks (Fig. 7) compared to the neat DPP-P (Fig. 4) pattern indicating more crystalline and ordered domains in the blend, which is important for hole transport. All these findings again suggest well selection of highly crystalline molecules is an important and essential method to improve the performance of M-P nonfullerene OSCs.

3. Experimental

3.1. General information

Nuclear magnetic resonance (NMR) spectra were obtained on Varian 400 MHz spectrometer. Mass spectra (MS) were obtained on Thermal Fisher Trace-ISQ spectrometer. UV–vis–NIR spectra were recorded on a Perkin Elmer model Lambda 750. Tapping-mode AFM images were obtained with a Veeco Multimode V instrument, 2D GIWAXS experiments were conducted at Shanghai Synchrotron Radiation Facility (SSRF) on a diffraction beam line (BL14B1). P(NDI2OD-T2) was prepared according to our previous report (M_n = 36.0 kDa, PDI = 2.5) [27]. All the chemicals were purchased from Sunatech Inc, Sigma-Aldrich and Strem Chemicals Inc. Toluene and DMF were purchased from Adamas Reagent. Ltd and distilled before use.

3.2. Synthesis of DPP-B

In a 50 mL reaction tube, 3,6-Bis(5-bromothien-2-yl)-2,5-bis(2-ethylhexyl)pyrrolo[3,4-c]pyrrole-1,4(2H,5H)-dione (210 mg, 0.4 mmol), bromobenzene (156 mg, 1.0 mmol), pivalic acid (4.6 mg, 0.02 mmol), were dissolved in 4 mL dry toluene under argon. After stirred at 110 °C for 4 h, the mixture was subsequently poured into ice water and extracted with chloroform and the combined extracts were dried with anhydrous Na_2SO_4 and evaporated. The crude product was purified by flash column chromatography on silica gel eluting using the mixture of CH_2Cl_2 and hexane to give DPP-B as dark purple solid. ^{1}H NMR (400 MHz, $CDCl_3$): δ (ppm) 9.00 (d, 2H), 8.20 (dd, 2H), 7.80–7.59 (m, 4 H), 7.62 (d, 2H), 7.60–7.57 (m, 4 H), 4.20–4.10 (m, 4H), 2.00 (s, 2H), 1 0.50–1.27 (m, 16H), 0.99–0.87 (m, 12 H); MS (m/z): $[M]^+$ calcd for $C_{42}H_{48}N_2O_2S_2$, 676.32; found, 676.46.

3.3. Synthesis of DPP-N

In a 50 mL reaction tube, 3,6-Bis(5-bromothien-2-yl)-2,5-bis(2-ethylhexyl)pyrrolo[3,4-c]pyrrole-1,4(2H,5H)-dione (210 mg, 0.4 mmol), 2-bromonaphthalene (207 mg, 1.0 mmol), pivalic acid (4.6 mg, 0.02 mmol), were dissolved in 4 mL dry toluene under argon. After stirred at 110 °C for 4 h, the mixture was subsequently poured into ice water and extracted with chloroform and the combined extracts were dried with anhydrous Na_2SO_4 and evaporated. The crude product was purified by flash column chromatography on silica gel eluting using the mixture of CHCl3 and hexane to give DPP-N as dark purple solid. ^{1}H NMR (400 MHz, $CDCl_3$): δ (ppm) 9.00 (d, 4H), 7.75–7.35 (m, 14 H), 4.20–4.05 (m, 4 H), 1.99 (s, 2H), 1.50–1.27 (m, 16H), 0.99–0.87 (m, 12 H); MS (m/z): $[M]^+$ calcd for $C_{50}H_{52}N_2O_2S_2$, 776.35; found, 776.10.

3.4. Synthesis of DPP-P

In a 50 mL reaction tube, 3,6-Bis(5-bromothien-2-yl)-2,5-bis(2-hexyldecyl)pyrrolo[3,4-c]pyrrole-1,4(2H,5H)-dione (362 mg, 0.4 mmol), 2 bromopyrene (281 mg, 1.0 mmol), pivalic acid (4.6 mg,

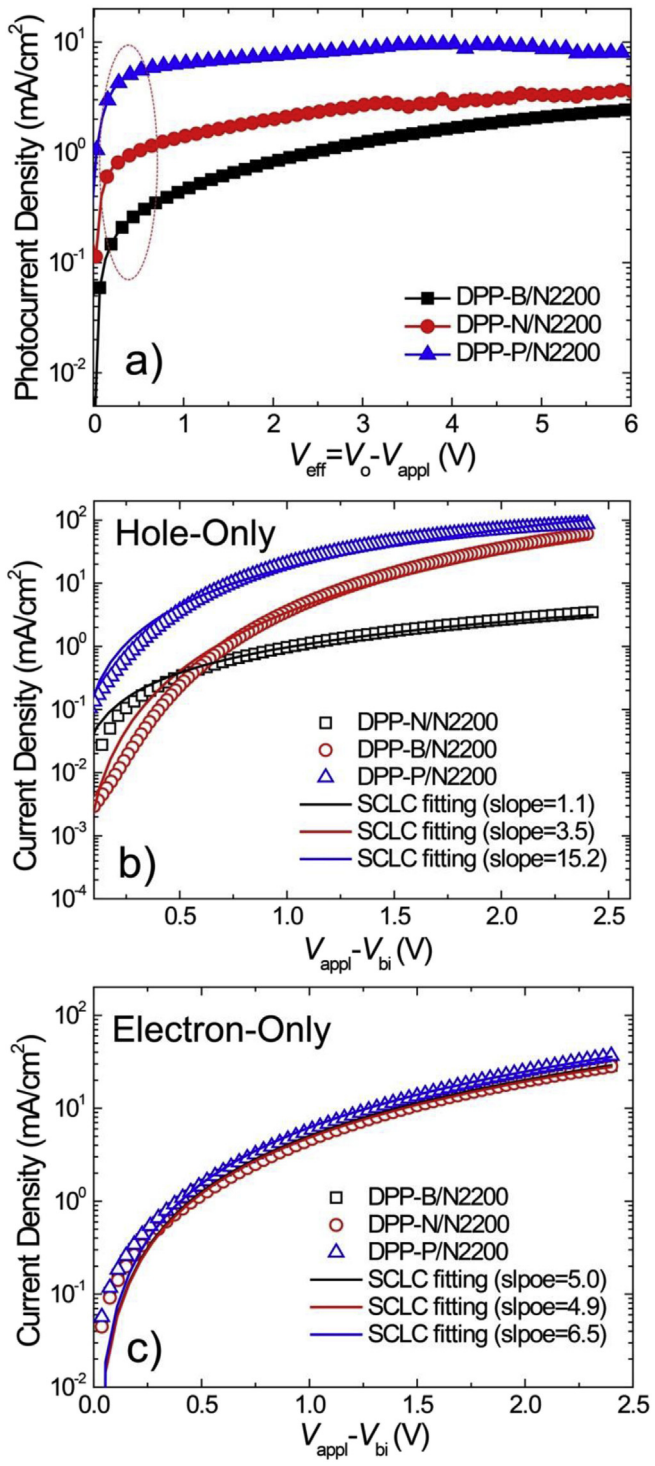

Fig. 5. Characteristics of photocurrent density (J_{ph}) versus effective voltage (V_{eff}) in optimal molecule/N2200 solar cell devices (a); *J-V* curves and SCLC fit of hole-only (b) and electron-on (c) diodes devices.

0.02 mmol), were dissolved in 4 mL dry toluene under argon. After stirred at 110 °C for 4 h, the mixture was subsequently poured into ice water and extracted with chloroform and the combined extracts were dried with anhydrous Na_2SO_4 and evaporated. The crude product was purified by flash column chromatography on silica gel eluting using the mixture of CHCl3 and hexane to give DPP-P as dark purple solid. ^{1}H NMR (400 MHz, $CDCl_3$): δ (ppm) 9.04 (d, 2H), 8.40 (s, 4H), 8.20 (d, 4 H), 8.10–7.95 (m, 8H), 4.20 (d, 4 H), 2.00 (m, 2H), 1.50–1.20 (m, 48 H), 0.90–0.75 (m, 12 H); MS (m/z): $[M]^+$ calcd for $C_{78}H_{88}N_2O_2S_2$, 1148.63; found, 1147.92.

3.5. Fabrication and characterization of polymer solar cells

Polymer solar cells were fabricated with a general structure of ITO/PEDOT:PSS (40 nm)/Active layer/Al (80 nm). Patterned ITO glass substrates were cleaned by sequential ultrasonic treatment in detergent, acetone, deionized water and isopropyl alcohol. The organic residue was further removed by treating with UV-ozone for 10 min. A thin film of PEDOT:PSS (Al 4083) was spin-coated on ITO substrates and dried at 150 °C for 10 min in ambient atmosphere. A blend of molecule/N2200 (ratio = 2/1, 16 mg/mL) was dissolved in chloroform w/wo 0.5% (v/v) diiodooctane, filtered through a 0.45 μm poly(tetrafluoroethylene) (PTFE) filter, spin-coated at 2000 rpm. Finally, 80 nm Al (2A/s) layers were thermally evaporated on the active layer at a pressure of 1.0×10^{-6} mbar through a shadow mask (active area 7.25 mm^2). The current density–voltage characteristics of the photovoltaic cells were measured using a Keithely 2400 (I–V) digital source meter under a simulated AM 1.5G solar irradiation at 100 mW/cm2 (Newport, Class AAA solar simulator, 94023A-U). The light intensity is calibrated by a certified Oriel Reference Cell (91150V) and verified with a NREL calibrated Hamamatsu S1787-04 diode.

3.6. Mobility measurements by space charge limited current (SCLC) method

Hole-only and electron-only devices were fabricated to measure the hole and electron mobility using the space charge limited current (SCLC) method. The hole-only device structure is ITO/PEDOT:PSS/polymer or blend/MoOx (6 nm)/Ag (80 nm) and the electron-only device structure is ITO/ZnO/polymer or blend/LiF (0.6 nm) /Al (80 nm). The thickness was measured by profilometer. The mobility was determined by fitting the dark current to the model of a single carrier SCLC, which is described by the equation:

$$J = \frac{9}{8}\varepsilon_0\varepsilon_r\mu_h\frac{V^2}{d^3},$$

Where J is the current, ε_0 is the permittivity of free space, ε_r is the relative permittivity of the material, μ is the zero-field mobility, d is the thickness of the polymer layer, V is the applied voltage. Then hole mobilities were calculated from the fitting slope of the $J^{1/2}$-Vcurves.

4. Conclusions

In order to specifically investigate the small molecule donor-polymer acceptor (M-P) nonfullerene solar cells, we have successfully modified the synthesis of a series of molecules containing a D-π-DPP-π-D backbone by the incorporation of different end groups (D) (benzene, naphthalene and pyrene), aiming to further improve the J_{sc} and *FF* of the M-P solar cells. Both experimental results and theoretical calculations have shown that the size of the end groups can fine-tune the polymer crystallinity and intermolecular packing by altering the molecular coplanarity. The molecule crystallinity, coplanarity and the use of additives play critical roles in improving the morphology of the M-P blend. By using commercially available n-type polymer N2200, the optimized solar cells demonstrated an increased FF of 58.5%, a V_{oc} of 0.78 V, a J_{sc} of ~4.5 mA/cm^2 and a PCE above 2.0%, which is among the highest efficiency reported for M-P nonfullerene OSCs. The synergetic effect of molecular crystallinity

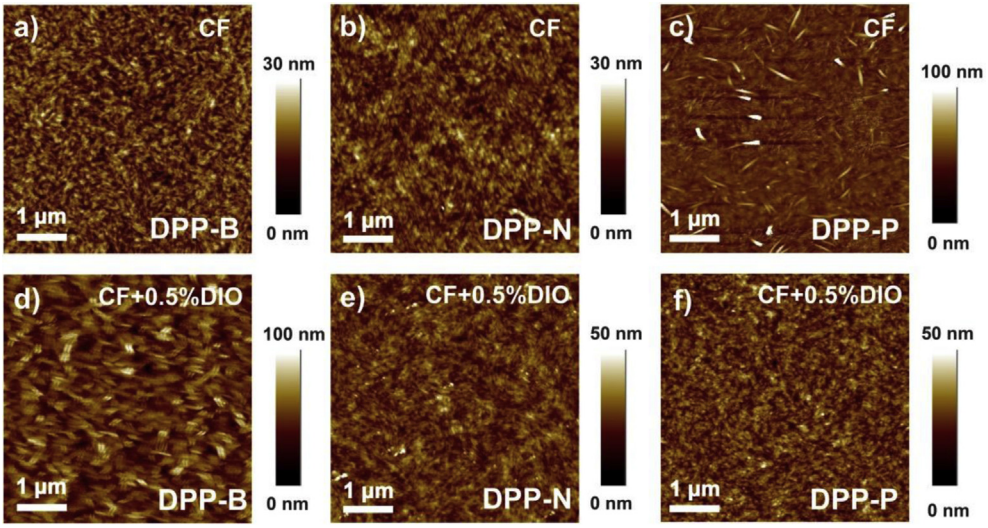

Fig. 6. AFM height images of PPT-PCBM DPP-B (a, d), DPP-N (b, e) and DPP-P (c, f) based blend films processed from chloroform w/wo DIO.

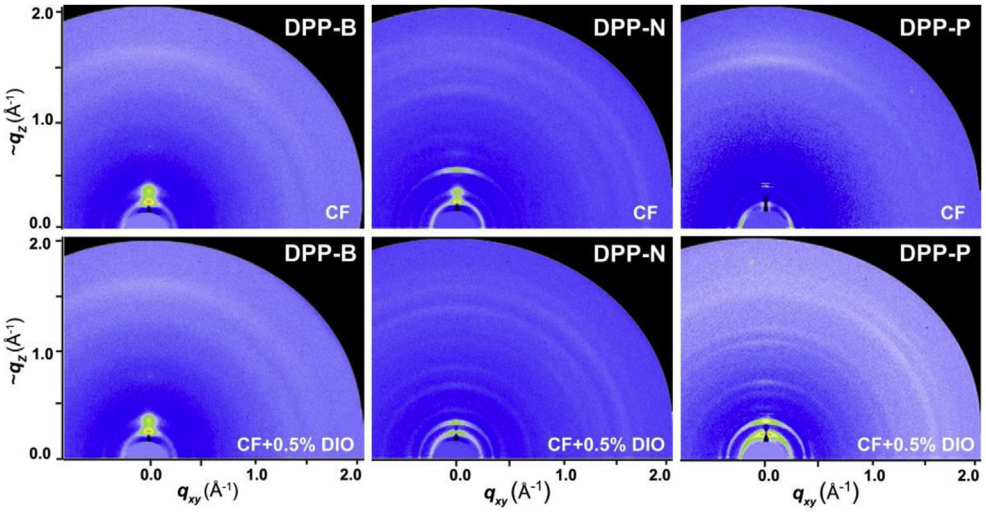

Fig. 7. 2D-GIWAXS patterns of PPT-PCBM DPP-B (a, d), DPP-N (b, e) and DPP-P (c, f) based blend films processed from chloroform w/wo DIO.

and processing additives on blend morphology makes it an efficient strategy to optimize the currently lower performance of M-P nonfullerene OSCs.

Acknowledgements

The author thanks the Collaborative Innovation Center of Suzhou Nano Science and Technology, Soochow University, Shanghai Synchrotron Radiation Facility (SSRF). This work was supported by the National Natural Science Foundation of China (Grant No. 61222401, No. 61674111). And we also acknowledge the Priority Academic Program Development of Jiangsu Higher Education Institutions (PAPD).

References

[1] a) G. Yu, J. Gao, J.C. Hummelen, F. Wudl, A.J. Heeger, Science 270 (1995) 1789;
b) B.C. Thompson, J.M.J. Fréchet, Angew. Chem. Int. Ed. 47 (2008) 58;
c) Y.F. Li, Acc. Chem. Res. 45 (2012) 723.
[2] a) J. You, L. Dou, K. Yoshimura, T. Kato, K. Ohya, T. Moriarty, K. Emery, C.-C. Chen, J. Gao, G. Li, Y. Yang, Nat. Commun. 4 (2013) 1446;
b) B. Kan, Q. Zhang, M. Li, X. Wan, W. Ni, G. Long, Y. Wang, X. Yang, H. Feng, Y. Chen, J. Am. Chem. Soc. 136 (2014) 15529;
c) Y. Liu, J. Zhao, Z. Li, C. Mu, W. Ma, H. Hu, K. Jiang, H. Lin, H. Ade, H. Yan, Nat. Commun. 5 (2014) 5293;
d) Z. He, B. Xiao, F. Liu, H. Wu, Y. Yang, S. Xiao, C. Wang, T.P. Russell, Y. Cao, Nat. Photonics 9 (2015) 174;
e) J. Zhao, Y. Li, G. Yang, K. Jiang, H. Lin, H. Ade, W. Ma, Nat. Energy 1 (2016) 15027.
[3] a) X. Zhan, Z. Tan, B. Domercq, Z. An, X. Zhang, S. Barlow, Y. Li, D. Zhu, B. Kippelen, S.R. Marder, J. Am. Chem. Soc. 129 (2007) 7246;
b) A. Facchetti, Mater. Today 16 (2013) 123;
c) S. Shi, J. Yuan, G. Ding, M. Ford, G. Shi, Yong Li, J. Sun, X. Ling, W. Ma, Adv. Funct. Mater. 26 (2016) 5669.
[4] a) J.M. Warman, M.P. de Haas, T.D. Anthopoulos, D.M. de Leeuw, Adv. Mater. 18 (2006) 2294;
b) W.Y. Huang, P.T. Huang, Y.K. Han, C.C. Lee, T.L. Hsieh, M.Y. Chang, Macromolecules 41 (2008) 7485;
c) T. Agostinelli, S. Lilliu, J.G. Labram, M.C. Quiles, M. Hampton, E. Pires, J. Rawle, O. Bikondoa, D.D.C. Bradley, T.D. Anthopoulos, J. Nelson, J.E. Macdonald, Adv. Funt. Mater. 21 (2011) 1701.
[5] a) C.C. Chueh, K. Yao, H.L. Yip, C.Y. Chang, Y.X. Xu, K.S. Chen, C.Z. Li, P. Liu, F. Huang, Y. Chen, W.C. Chen, A.K.-Y. Jen, Energy Environ. Sci. 6 (2013) 3241;
b) Y. Chen, S. Zhang, Y. Wu, J. Hou, Adv. Mater. 26 (2014) 2744;
c) X. Chen, X. Liu, M.A. Burgers, Y. Huang, G.C. Bazan, Angew. Chem. Int. Ed. 53 (2014) 14378.
[6] a) Y.J. Cheng, S.H. Yang, C.S. Hsu, Chem. Rev. 109 (2009) 5868;
b) H. Burckstummer, A. Weissenstein, D. Bialas, F. Wurthner, J. Org. Chem. 76

(2011) 2426;
c) B. Carsten, F. He, H.J. Son, T. Xu, L. Yu, Chem. Rev. 111 (2011) 1528.
[7] a) M. Lafrance, C.N. Rowley, T.K. Woo, K. Fagnou, J. Am. Chem. Soc. 128 (2006) 8754;
b) M. Lafrance, K. Fagnou, J. Am. Chem. Soc. 128 (2006) 16496.
[8] a) Y. Tan, J.F. Hartwig, J. Am. Chem. Soc. 133 (2011) 3308;
b) P. Berrouard, A. Najari, A. Pron, D. Gendron, P.O. Morin, J.-R. mi Pouliot, J. Veilleux, M. Leclerc, Angew. Chem. In. Ed. 51 (2012) 2068;
c) W. Zhang, A.J. Chen, E.V. Rojas, T.V. Jucov, T.C. Timofeeva, S. Parker, S.R. Barlow, Marder, J. Am. Chem. Soc. 135 (2013) 16376.
[9] a) Y. Lin, Q. He, F. Zhao, L. Huo, J. Mai, X. Lu, C. Su, T. Li, J. Wang, J. Zhu, Y. Sun, C. Wang, X. Zhan, J. Am. Chem. Soc. 138 (2016) 2973;
b) Y. Lin, F. Zhao, Q. He, L. Huo, Y. Wu, T.C. Parker, W. Ma, Y. Sun, C. Wang, D. Zhu, A.J. Heeger, S.R. Marder, X. Zhan, J. Am. Chem. Soc. 138 (2016) 4955;
c) W. Zhao, D. Qian, S. Zhang, S. Li, O. Inganäs, F. Gao, J. Hou, Adv. Mater. 2016, 28, 4734; d) S. Li, L. Ye, W. Zhao, S. Zhang, S. Mukherjee, H. Ade, J. Hou, Adv. Mater. (2016), http://dx.doi.org/10.1002/adma.201602776.
[10] a) T. Kim, J.-H. Kim, T.E. Kang, C. Lee, H. Kang, M. Shin, C. Wang, B. Ma, U. Jeong, T.-S. Kim, B.J. Kim, Nat. Commun. 6 (2015) 8547;
b) L. Gao, Z.G. Zhang, L. Xue, J. Min, J. Zhang, Z. Wei, Y. Li, Adv. Mater. 28 (2015) 1884;
c) J. Sun, J. Gu, J. Yuan, K. Lu, Sh Shi, W. Ma, Org. Electron. 33 (2016) 227.
[11] a) O.K. Kwon, J.-H. Park, D.W. Kim, S.K. Park, S.Y. Park, Adv. Mater. 27 (2015) 1951;
b) J. Min, O.K. Kwon, C. Cui, J.-H. Park, Y. Wu, S.Y. Park, Y. Li, C.J. Brabec, J. Mater. Chem. A (2016), http://dx.doi.org/10.1039/C6TA05303C.
[12] a) Z. Li, J.D.A. Lin, H. Phan, A. Sharenko, C.M. Proctor, P. Zalar, Z. Chen, A. Facchetti, T.-Q. Nguyen, Adv. Funct. Mater. 24 (2014) 6989;
b) Z. Tang, B. Liu, A. Melianas, J. Bergqvist, W. Tress, Q. Bao, D. Qian, O. Inganäs, F. Zhang, Adv. Mater. 27 (2015) 1990.
[13] J.W. Jung, T.P. Russell, W.H. Jo, Chem. Mater. 27 (2015) 4865.
[14] a) D. Mori, H. Benten, I. Okada, H. Ohkita, S. Ito, Energy Environ. Sci. 7 (2014) 2939;
b) J.R. Moore, S. Albert-Seifried, A. Rao, S. Massip, B. Watts, D.J. Morgan, R.H. Friend, C.R. McNeill, H. Sirringhaus, Adv. Energy Mater. 1 (2011) 230.
[15] H. Yan, Z. Chen, Y. Zheng, C. Newman, J.R. Quinn, F. Dötz, M. Kastler, A. Facchetti, Nature 457 (2009) 679.
[16] S.-Y. Liu, M.-M. Shi, J.-C. Huang, Z.-N. Jin, X.-L. Hu, J.-Y. Pan, H.-Y. Li, A.K.-Y. Jen, H.-Z. Chen, J. Mater. Chem. A 1 (2013) 2795.
[17] a) Y. Liu, X. Du, Z. Xiao, J. Cao, S. Tan, Q. Zuo, L. Ding, Syn. Met. 162 (2012) 1665;
b) O.P. Lee, A.T. Yiu, P.M. Beaujuge, C.H. Woo, T.W. Holcombe, J.E. Millstone, J.D. Douglas, M.S. Chen, J.M.J. Fréchet, Adv. Mater. 23 (2011) 5359.
[18] J. Yuan, Z. Zhai, J. Li, J. Lu, X. Huang, Z. Xu, W. Ma, J. Mater. Chem. A 1 (2013) 12128.
[19] R.L. Uy, S.C. Price, W. You, Macromol. Rapid Comm. 33 (2012) 1162.
[20] J. Rivnay, S.C.B. Mannsfeld, C.E. Miller, A. Salleo, M.F. Toney, Chem. Rev. 112 (2012) 5488.
[21] a) D.P. McMahon, D.L. Cheung, A. Troisi, J. Phys. Chem. Lett. 2 (2011) 2737;
b) F.C. Jamieson, E.B. Domingo, T. McCarthy-Ward, M. Heeney, N. Stingelin, J.R. Durrant, Chem. Sci. 3 (2012) 485;
c) H. Tamura, I. Burghardt, J. Am. Chem. Soc. 135 (2013) 16364.
[22] M. Schubert, B.A. Collins, H. Mangold, I.A. Howard, W. Schindler, K. Vandewal, S. Roland, J. Behrends, F. Kraffert, R. Steyrleuthner, Z. Chen, K. Fostiropoulos, R. Bittl, A. Salleo, A. Facchetti, F. Laquai, H. Ade, D. Neher, Adv. Funct. Mater. 24 (2014) 4068.
[23] a) W. Ma, C. Yang, X. Gong, K. Lee, A.J. Heeger, Adv. Funct. Mater. 15 (2005) 1617;
b) J.K. Lee, W.L. Ma, C.J. Brabec, J.S. Moon, J.Y. Kim, K. Lee, G.C. Bazan, A.J. Heeger, J. Am. Chem. Soc. 130 (2008) 3619;
c) S.J. Lou, J.M. Szarko, T. Xu, L. Yu, T.J. Marks, L.X. Chen, J. Am. Chem. Soc. 133 (2011) 20661;
d) X. Guo, C. Cui, M. Zhang, L. Huo, Y. Huang, J. Hou, Y. Li, Energy Environ. Sci. 5 (2012) 7943;
e) Y. Sun, G.C. Welch, W.L. Leong, C.J. Takacs, G.C. Bazan, A.J. Heeger, Nat. Mater. 11 (2012) 44.
[24] a) V.D. Mihailetchi, L.J.A. Koster, J.C. Hummelen, P.W.M. Blom, Phys. Rev. Lett. 93 (2004) 216601;
b) V.D. Mihailetchi, H.X. Xie, B. de Boer, L.J.A. Koster, P.W.M. Blom, Adv. Funct. Mater. 16 (2006) 699.
[25] a) A. Rose, Phys. Rev. 97 (1955) 1538;
b) M.A. Lampert, P. Mark, Current Injection in Solids, Academic, New York, 1970.
[26] a) J. Yuan, X. Huang, F. Zhang, J. Lu, Z. Zhai, C. Di, Z. Jiang, W. Ma, J. Mater. Chem. 22 (2012) 22734;
b) J. Yuan, Z. Zhai, H. Dong, J. Li, Z. Jiang, Y. Li, W. Ma, Adv. Funct. Mater. 23 (2013) 885.
[27] J. Yuan, W. Ma, J. Mater. Chem. A 3 (2015) 7077.